AGU PUBLICATIONS

Geophysical Research Letters

RESEARCH LETTER
10.1002/2016GL069841

Key Points:
- Hector Mine near-field surface deformation measured from air photo correlation is compared to Landers deformation (Milliner et al., 2015)
- Landers and Hector Mine had significant distributed deformation 46% and 39% over average fault widths of 154 m and 121 m, respectively
- Field measurements underestimate fault slip due to distributed strain thus affecting empirical scaling laws and geologic slip rates

Supporting Information:
- Supporting Information S1
- Table S1
- Table S2
- Table S3
- Table S4
- Table S5
- Table S6

Correspondence to:
C. W. D. Milliner,
milliner@berkeley.edu

Citation:
Milliner, C. W. D., J. F. Dolan, J. Hollingsworth, S. Leprince, and F. Ayoub (2016), Comparison of coseismic near-field and off-fault surface deformation patterns of the 1992 M_w 7.3 Landers and 1999 M_w 7.1 Hector Mine earthquakes: Implications for controls on the distribution of surface strain, *Geophys. Res. Lett.*, *43*, 10,115–10,124, doi:10.1002/2016GL069841.

Received 1 JUN 2016
Accepted 25 AUG 2016
Accepted article online 31 AUG 2016
Published online 7 OCT 2016

Comparison of coseismic near-field and off-fault surface deformation patterns of the 1992 M_w 7.3 Landers and 1999 M_w 7.1 Hector Mine earthquakes: Implications for controls on the distribution of surface strain

C. W. D. Milliner[1], J. F. Dolan[1], J. Hollingsworth[2,3], S. Leprince[4], and F. Ayoub[4]

[1]Department of Earth Sciences, University of Southern California, Los Angeles, California, USA, [2]ISTerre, Université Grenoble Alpes, Grenoble, France, [3]ISTerre, CNRS, Grenoble, France, [4]Division of Geological and Planetary Sciences, California Institute of Technology, Pasadena, California, USA

Abstract Subpixel correlation of preevent and postevent air photos reveal the complete near-field, horizontal surface deformation patterns of the 1992 M_w 7.3 Landers and 1999 M_w 7.1 Hector Mine ruptures. Total surface displacement values for both earthquakes are systematically larger than "on-fault" displacements from geologic field surveys, indicating significant distributed, inelastic deformation occurred along these ruptures. Comparison of these two data sets shows that 46 ± 10% and 39 ± 22% of the total surface deformation were distributed over fault zones averaging 154 m and 121 m in width for the Landers and Hector Mine events, respectively. Spatial variations of distributed deformation along both ruptures show correlations with the type of near-surface lithology and degree of fault complexity; larger amounts of distributed shear occur where the rupture propagated through loose unconsolidated sediments and areas of more complex fault structure. These results have basic implications for geologic-geodetic rate comparisons and probabilistic seismic hazard analysis.

1. Introduction

Analysis of recent coseismic surface ruptures reveals significant distributed, inelastic, off-fault deformation (OFD), ranging from completely diffuse to highly localized (i.e., between 0 and 100% of the observable total surface deformation being accommodated on the primary rupture strand) [e.g., *Rockwell et al.*, 2002; *Quigley et al.*, 2012; *Zinke et al.*, 2014; *Gold et al.*, 2015; *Milliner et al.*, 2015; *Teran et al.*, 2015]. Such inelastic surface deformation can be accommodated via a range of physical mechanisms, such as warping, granular flow, rigid-block rotation, and/or microcracking [*Nelson and Jones*, 1987; *Shelef and Oskin*, 2010]. However, how the magnitude of inelastic deformation may vary along the full length of a surface rupture and between events is poorly understood. Limiting this understanding is the dearth of comparative analyses of multiple earthquakes that can resolve near-field strain to the same precision and scale, which necessarily involves using data of comparable resolution, as well as equivalent measurement methods (e.g., geologic field surveys, 3-D topographic cloud matching, or optical image correlation), which can otherwise yield arbitrary differences in the amount of observable deformation. For example, for the 2013 M_w 7.7 Balochistan earthquake, *Zinke et al.* [2014] reported 45% OFD, whereas *Gold et al.* [2015] found 28%, a disagreement attributed to differences in measurement and sampling of displacement, and satellite resolution (see further explanation in supporting information Text S4). Accurately understanding the degree of strain localization and whether there exist systematic differences or similarities between different earthquakes is key to help understand fault mechanics, the geologic evolution of fault systems, and developing effective microzonation protocols for the built environment.

Here we use subpixel image correlation applied to pairs of before-and-after, high-resolution air photos of the 1999 M_w 7.1 Hector Mine earthquake to analyze the near-field surface deformation pattern and quantify the amount of inelastic, distributed deformation along the surface rupture. For the 1999 Hector Mine earthquake we used the same optical image correlation method (COSI-Corr) and air photos as that used in the analysis of the 1992 Landers earthquake by *Milliner et al.* [2015], therefore providing for the first time a robust comparative analysis of near-field surface deformation patterns between two earthquakes to the same precision and resolution along their full rupture lengths. Along the M_w 7.3 1992 Landers surface rupture, 46 ± 10% of the

total surface shear was accommodated as OFD over average fault zone widths of 154 m, and the spatial variation of OFD could be explained by variations in the macroscopic geometrical structural complexity, but with no clear correlation with the types of near-surface materials [*Milliner et al*., 2015]. Both the Landers and Hector Mine events ruptured systems of structurally immature faults (cumulative displacement of 3-7 km [*Jachens et al*., 2002]) within the Eastern California Shear Zone (ECSZ) of the Mojave Desert, California, an 80 km wide region of NNW orientated, right-lateral shear.

Herein we seek to understand whether there are common features or systematic differences in the amount of inelastic deformation between the two surface ruptures, and what physical properties of the rupture may explain variations between these two seemingly similar events. We discuss our results in light of their implications for understanding discrepancies between geodetic and geologic slip rates across the ECSZ, the accuracy of empirical scaling relations of earthquake surface ruptures derived from field measurements, and use of such data for probabilistic seismic hazard analysis.

2. Data and Methods

To measure the near-field, horizontal surface deformation pattern of the Hector Mine earthquake, we used the program COSI-Corr (coregistration of optically sensed images and correlation), which allows for accurate coregistration, orthorectification, and correlation of pairs of preevent and postevent optical images to subpixel precision [*Leprince et al*., 2007a, 2007b]. We selected 21 pairs of 1 m resolution National Aerial Photography Program (NAPP) aerial photos for correlation (from http://earthexplorer.usgs.gov/), acquired from July 1994 to May 2002, which cover the entire length of the Hector Mine surface rupture. We produced the deformation maps following the approach described in *Milliner et al*. [2015], using the same type of imagery (NAPP air photos), resolution (1 m), digital elevation model (10 m, 2012 National Elevation Dataset DEM), correlation method (COSI-Corr phase correlator), and correlation window parameters (a multiscale window size of 64×64 pixels (initial correlation) and 32×32 pixels (final correlation), with a step of six pixels across the image). This procedure generated deformation maps of the same resolution (6 m) and comparable precision (10 cm root mean square (one tenth of the input image pixel size)) as for the Landers result [*Milliner et al*., 2015].The horizontal fault displacement and fault zone width (FZW) are measured from the correlation maps using fault-perpendicular stacked profiles (lengths of 1–3 km; widths of 138 m) in the same manner outlined in *Milliner et al*. [2015], where a straight line is manually fit to either side of the fault and extrapolated to the fault trace to approximate the total amplitude and width of the coseismic offset (Figure 1b and see supporting information Text S2 and Figures S7 and S8). The COSI-Corr "displacement" measurement thus includes both the localized, on-fault displacement, and any distributed inelastic shear accommodated across the entire width of the fault zone.

We estimated OFD along the 1999 Hector Mine rupture by differencing the nearest geologic field measurements (which captures the on-fault, discrete component of slip) from our displacement measurements (which captures the total displacement), the same approach employed for Landers [*Milliner et al*., 2015] (see supporting information Text S4). Field survey measurements are assumed to primarily capture the discrete, on-fault component of slip because they typically use piercing points taken over a narrow (1–10 m wide) fault-perpendicular aperture and therefore usually do not (and frequently cannot) include precise measurement of the complex, distributed off-fault deformation [*McGill and Rubin*, 1999; *Rockwell et al*., 2002]. For measurements that capture the "on-fault," discrete component of horizontal displacement, we used 136 field measurements [*Treiman et al*., 2002] and 255 measurements derived from a postevent lidar DEM [*Chen et al*., 2015].

3. Results

The Hector Mine correlation maps reveal a complex system of 22 interconnected right-lateral, NNW orientated fault segments with a total rupture length of 45 km (Figure 1). From the correlation maps we extracted 470 measurements of fault displacement and 443 measurements of FZW (synthetic tests show that these measurements are not biased by long-wavelength ($>$1 km) geometrical artifacts, such as thermomechanical warping of the film and scanning artifacts, that occur within the correlation maps [see *Michel and Avouac*, 2006; *Ayoub et al*., 2009; *Milliner et al*., 2015]). Measurements of displacement follow an exponential distribution, with a mean displacement of 2.84 m, median of 3.04 m, and a maximum slip of 5.51 m, located in the Bullion Mountains 7 km south of the epicenter (see supporting information Text S1 and Figure S6 for comparison of these measurements with

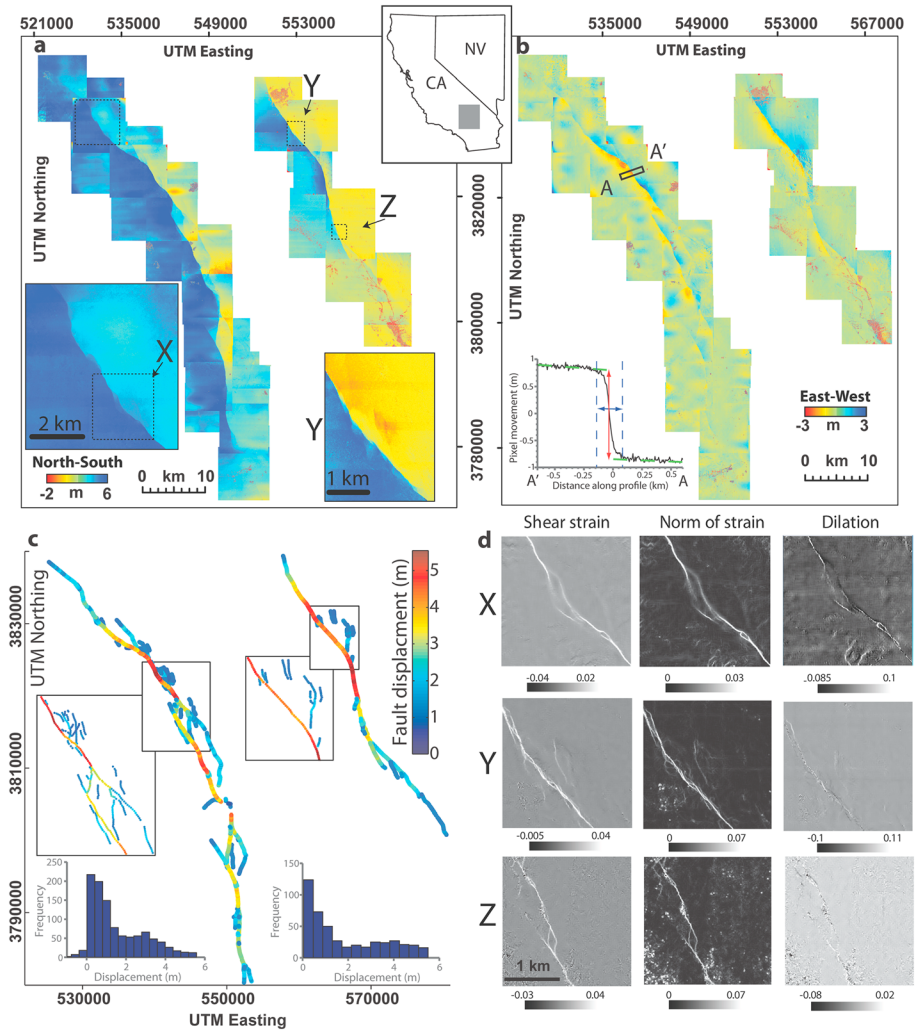

Figure 1. Correlation maps of the 1992 Landers and 1999 Hector Mine earthquakes. (a and b) North-south and east-west component of surface motion, respectively, with region of study shown by gray box within inset, top right of Figure 1a. Inset in lower left of Figure 1b shows fault-parallel displacement (black line) within a 138 m wide stacked profile, illustrating how fault offset (red vertical arrow) and fault zone width (blue horizontal arrow) are measured using linear regressions (green dashed lines). (c) Displacement measurements from the correlation maps, 1058 measurements for Landers and 470 for Hector Mine. (d) Strain maps computed from the correlation maps (labeled X, Y, Z). Left column shows shear strain, middle, norm of 2-D strain tensor and right, dilation. Top row shows transtensional step over along Landers rupture (location outlined by dashed box within inset of Figure 1a) and middle and bottom rows show area of distributed deformation and transtensional step over along Hector Mine (outlined by dashed boxes in a); these examples illustrate distributed deformation along rupture.

those from SPOT correlations). Measurements of the FZW follow an exponential distribution with a mean value of 121 m, median of 84 m, and a maximum fault width of 876 m, found at the southern termination of the rupture. The FZW is notably wider in areas of geometrical fault complexities, such as in the southern central segment (13.5 km south of the epicenter, where the Bullion Mountain fault branches into the Lavic Lake fault), 3.5 km south of the epicenter where the main fault bifurcates, at a ~18° bend along the central segment of the Lavic Lake fault, and at the southern termination of the rupture with 300–876 m of highly distributed shear.

To visualize the distributed nature of strain along 1999 Hector Mine surface rupture, we computed the 2-D strain field from the correlation maps using a central difference method that is first-order accurate. The strain maps show how shear strain systematically increases and dilation (trace of the strain tensor) decreases in areas of simple fault structure where deformation is localized to narrow fault cores, and vice versa at sites of geometrical structural complexity, such as fault branches, kinks, bends, and step overs (Figure 1d). The

strain maps illustrate the difficulty of incorporating such diffuse deformation in measurements taken from offset geomorphic features close to the primary fault strand, as is typically performed in traditional field and lidar analysis of surface ruptures [e.g., *Sieh et al*., 1993; *Chen et al*., 2015].

Comparison of the field and lidar "on-fault" measurements of fault slip with our COSI-Corr "total displacement" measurements shows that the latter are systematically larger (Figures 2e and 2f), revealing the spatial variation of OFD at 220 points along the length of the Hector Mine surface rupture. From this differencing we found a mean OFD of 1.29 m (estimated from both the field and lidar measurements) and median of 1.01 m. Normalizing each OFD point by the corresponding total displacement from our COSI-Corr measurements (as displacement itself varies along the rupture) gives the percent of off-fault deformation (OFD%), reflecting the relative magnitude of OFD compared to the total deformation accommodated at a point across the fault zone. We found the mean OFD% for the Hector Mine surface rupture of 41 ± 25% (1σ, $n = 86$) and 38 ± 17% (1σ, $n = 134$), derived from comparison with the field and lidar measurements, respectively, giving an overall mean OFD% of 39 ± 22% (1σ, $n = 220$). Qualitatively, the estimates of OFD from the field and lidar data sets both exhibit similar spatial variations along the rupture length (Figure 2b). To a first order, OFD is lowest in the central segment of the rupture, coincident with the bedrock exposed in the Bullion Mountains, and generally increases to the north and south, where the rupture passed through surficial unconsolidated Quaternary sediments. Although our displacement measurements likely include some postseismic afterslip because the postevent images were acquired three years after the Hector Mine event, the effect is likely minor, as interferometric synthetic aperture radar measurements collected 1 year following the earthquake detected only 6 cm of surface afterslip [*Jacobs et al*., 2002], a level below our threshold of detection (10 cm), and postseismic velocities from GPS found similarly small levels of motion [*Agnew et al*., 2002; *Hudnut et al*., 2002; *Owen et al*., 2002].

4. Discussion and Conclusions

Our use of the same correlation method and equivalent imagery to quantify the near-field deformation of the 1999 Hector Mine earthquake as that used by *Milliner et al*. [2015] to document the 1992 Landers event allows us to resolve surface deformation to the same resolution and degree of accuracy, thus facilitating a robust comparison of the magnitude and spatial variation of inelastic surface deformation in these events. For the Landers and Hector Mine surface ruptures we found similar magnitudes of distributed deformation, with 46 ± 10% (1σ) and 39 ± 22% (1σ) total surface shear distributed away from the primary fault strand, respectively. These high percentages are consistent with the structural immaturity of the two fault systems (both with cumulative displacements of 3–7 km [*Jachens et al*., 2002]), and similar values of distributed deformation have been documented along other structurally immature faults [e.g., *Quigley et al*., 2012; *Zinke et al*., 2014; *Gold et al*., 2015].

Although the similar structural immaturity of the faults that ruptured in the Landers and Hector Mine events likely explains the overall large percentages of OFD, spatial variations of OFD along both surface ruptures indicate there are likely other, secondary physical controls at work. We explore this by investigating how the magnitude of distributed strain varies as a function of observable properties along the surface rupture (e.g., the type of near-surface materials and macroscopic local fault zone structural complexity), testing the hypothesis that less consolidated materials and more geometrically complex fault zones produce larger magnitudes of distributed strain.

OFD along the Landers rupture from *Milliner et al*. [2015] was found to be large in areas of unconsolidated Quaternary sediments (mean OFD of 49 ± 24% [1σ]), lowest at sites where sediment is juxtaposed against bedrock (positively skewed distribution with a mode of 19%), and unexpectedly large in areas of bedrock (mean of 52 ± 25% [1σ]), (Figure 3). The relatively discrete deformation occurring at sites of sediment-bedrock interfaces suggests that these preexisting mechanical interfaces act to localize deformation, as has been found from field investigations and dynamic rupture simulations [*Chester and Logan*, 1986; *Bruhn et al*., 1994; *Ben-Zion and Sammis*, 2003; *Sibson*, 2003]. However, although it seems counterintuitive that OFD was largest in areas of bedrock, the majority of bedrock exposed along the Landers surface rupture (82%) crops out within the structurally complex junction between the Emerson and Homestead Valley faults, where significant dip-slip faulting occurs within a transtensional step over that has locally exhumed bedrock. Thus, the interdependency of macroscopic fault zone complexity and material type makes it particularly

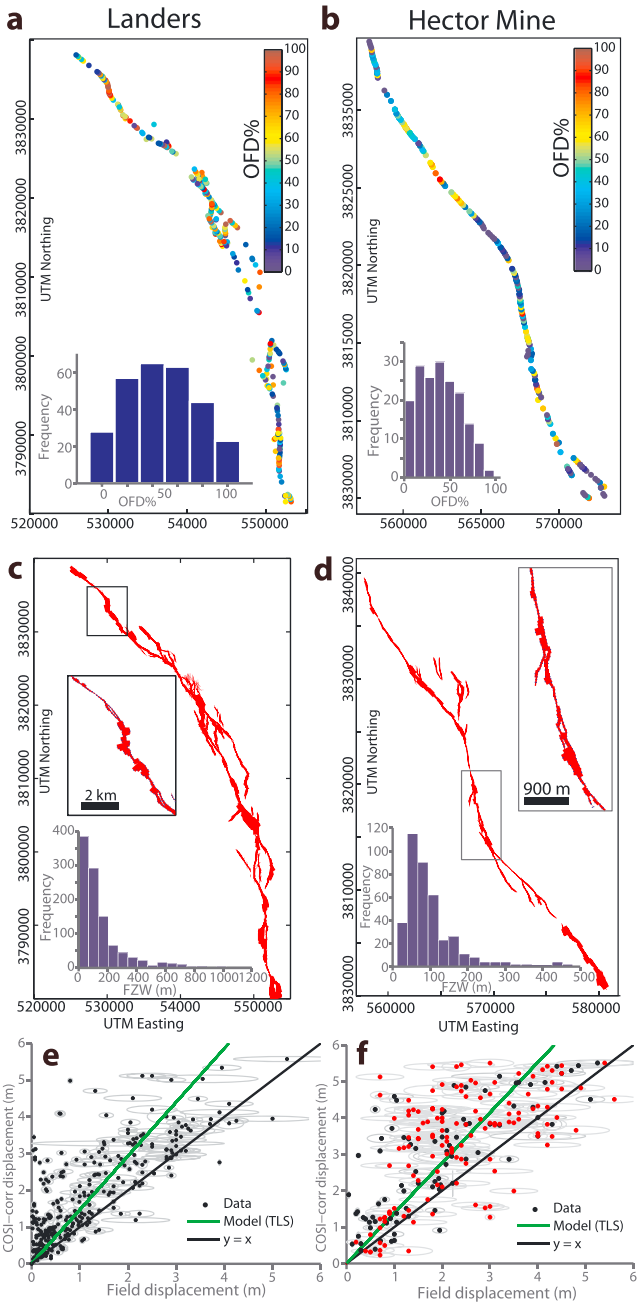

Figure 2. (a and b) Off-fault deformation and (c and d) fault zone width measurements for Landers and Hector Mine. Figure 2a show OFD as a percent (OFD%) is computed for Landers by differencing COSI-Corr measurements from field values [*Sieh et al.*, 1993], result from *Milliner et al.* [2015], and for Hector Mine differencing from both the field [*Treiman et al.*, 2002] and lidar measurements [*Chen et al.*, 2015]. Figures 2c and 2d show the map view of fault zone width (FZW) measurements (red lines) measured from the stacked profiles, spaced every 138 m. Inset images shows examples where the FZW increases where the rupture becomes structurally complex (e.g., at branches, bends, or terminations). (e and f) Correlation plots showing the systematic difference of COSI-Corr displacement measurements versus those from field surveys [*Sieh et al.*, 1993] for Landers and from field (black dots [*Treiman et al.*, 2002]) and lidar measurements (red dots [*Chen et al.*, 2015]) for Hector Mine. Total least squares regression (green line) to the data (gray ellipses indicate 1σ error) has gradient of 1.47, with R^2 of 0.77 for Landers and gradient of 1.38 and R^2 of 0.84 for Hector Mine, both in contrast to the $y = x$ (black lines) indicating OFD.

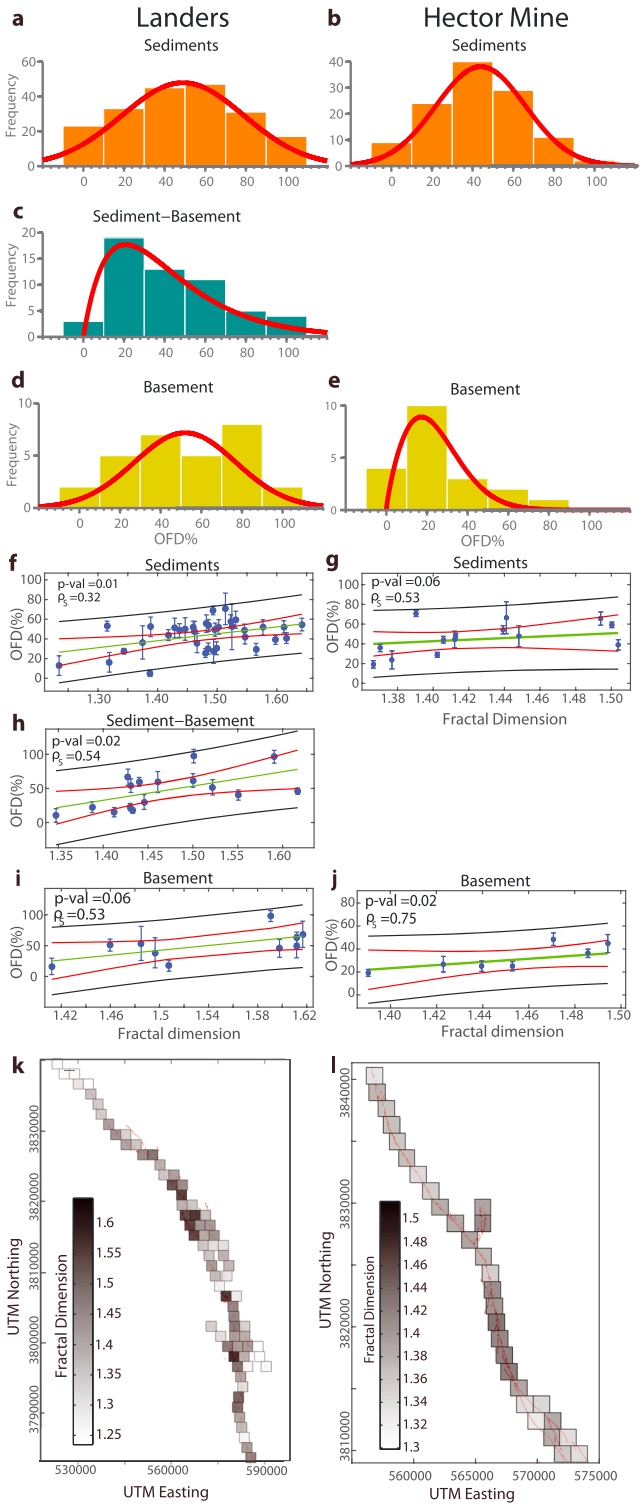
a
Landers
Sediments
Frequency
b
Hector Mine
Sediments
c
Sediment–Basement
Frequency
d
Basement
Frequency
OFD%
e
Basement
OFD%
f
Sediments
p-val =0.01
ρs =0.32
OFD(%)
g
Sediments
p-val =0.06
ρs =0.53
OFD(%)
Fractal Dimension
h
Sediment–Basement
p-val =0.02
ρs =0.54
OFD(%)
i
Basement
p-val =0.06
ρs =0.53
OFD(%)
Fractal dimension
j
Basement
p-val =0.02
ρs =0.75
OFD(%)
Fractal dimension
k
UTM Northing
Fractal Dimension
UTM Easting
l
UTM Northing
Fractal Dimension
UTM Easting

Figure 3

difficult to assess the relative effect of each of these parameters separately. In contrast, the simpler rupture pattern for Hector Mine and the binary distribution of materials along the rupture (Tertiary bedrock in the central 10 km of the rupture and unconsolidated Quaternary sediments to the north and south) allows us to better isolate and more clearly observe the effect of near-surface material type on the degree of strain localization. From the Hector Mine rupture, we found distinct differences of OFD with the type of material, with a mean OFD of 45% for sediments and a positively skewed distribution toward significantly lower OFD (mode of 20%) where the rupture propagated through bedrock (Figure 3).

To test the effect of macroscopic fault zone structural complexity on the magnitude of distributed deformation for both earthquakes, we quantified the degree of geometrical fault complexity using a box counting method that determines the fractal dimension of 1.5 km long segments of the mapped surface rupture (Figures 3k and 3l) [*Turcotte*, 1997]. Although the macroscopic fault zone organization cannot explain all of the variance in the OFD data (as shown by low R^2 values ranging from 0.26 to 0.68, and Spearman's rank correlations ranging from 0.32 and 0.75, for both ruptures), there is a statistically significant, general first-order positive correlation as evinced by p values ranging from 0.01 to 0.05. However, we do not expect fault zone geometrical complexity (or near-surface materials) alone to explain all of the variance in the observed OFD data (where some of the scatter is also likely due to noise from measurement uncertainty). The remaining, unexplained spatial variation of OFD could be attributed to other parameters not considered here, such as the thickness of sediment, fault dip, the state of stress, or the available fracture energy of the propagating rupture front, properties that should be considered in analysis of future surface ruptures. We envision that this type of analysis will serve as a useful template to better constrain these types of empirical scaling relations, eventually allowing for accurate a priori assessment and estimation of the expected amounts and patterns of OFD along a given mapped fault segment.

Geologic slip rates are commonly measured from restoration of offset geomorphic features (e.g., river channels), over narrow fault-perpendicular distances ($<$10 m) where confidence of the offset geometry is greatest. Such measurements are, however, susceptible to missing distributed strain, which can result in an underestimation of the long-term slip rate [e.g., *Dolan and Haravitch*, 2014; *Gold et al*., 2015]. For example, across the ECSZ, a system of six structurally immature faults, geologic rates are only about half of the geodetic rates, with rates of $\leq 6.2 \pm 1.9$ mm/yr [*Oskin et al*., 2008] and 12 ± 2 mm/yr [*Bennett et al*., 2003; *Meade and Hager*, 2005], respectively. Slip rates for the Camp Rock and Pisgah-Bullion faults (segments of the Landers and Hector Mine ruptures, respectively) were measured from offset of an alluvial terrace and a pyroclastic deposit, respectively, over $<$ 10 m wide, fault-perpendicular distances [*Oskin et al*., 2008]. Assuming the distributed coseismic deformation we observe is reflective of the long-term behavior (where we note that offset geologic markers along the neighboring Harper Lake fault indicate a similar long-term, "geologic OFD" of 45% [*Shelef and Oskin*, 2010]), such narrow-aperture geologic rates would likely be underestimated by such an amount. Correcting the geologic slip rates for 39–45% missed OFD for the six main faults that comprise the ECSZ would yield rates of 10–11.5 mm/yr, in agreement within 1σ uncertainty of the current geodetic rates. This implies that the apparent geologic-geodetic slip rate discrepancy, and therefore strain transient across the ECSZ (a current period of elevated shear loading argued to explain the rate mismatch), is much smaller than previously suggested [e.g., *Dolan et al*., 2007; *Oskin et al*., 2008]. This example illustrates the necessity of including OFD in all such geologic-geodetic rate comparisons.

Underestimation of the total surface displacement from field surveys due to missed distributed strain also has basic implications for empirical scaling laws relating mean displacement (D_{mean}) to M_w and rupture

Figure 3. Off-fault deformation (OFD) as a function of types of near-surface materials (Figures 3a–3e), with distribution fits (red lines), and fault zone complexity (Figures 3f–3j), for Landers and Hector Mine, in left and right column, respectively. (a and b) OFD in areas where the rupture propagated through sediment, exhibited large mean values of OFD of $49 \pm 24\%$ and $42 \pm 21\%$ for Landers and Hector Mine, respectively. (c) Histogram of OFD in areas of sediment-bedrock interfaces (only found along Landers rupture), with a positively skewed distribution (mode of 19%). (d and e) Histogram of OFD in areas of bedrock, with surprisingly large values of $52 \pm 25\%$ for Landers and significantly lower values for Hector Mine $29 \pm 20\%$. (f and g) OFD where the rupture propagated through sediment as a function of fault complexity (determined by the fractal dimension of 1.5 km segments of the fault trace, see Figures 3k and 3l). Higher fractal values denote more complex fault zones. Spearman rank correlation (ρ_s) and p values (p-val) are labeled in top left. (h) OFD versus fault complexity for Landers in sediment-bedrock areas. (i and j) OFD versus fault complexity in areas of bedrock only. (k and l) Box counting results illustrating areas of geometrical fault complexity of faults mapped from field surveys [*Bryant*, 1992; *Sieh et al*., 1993; *Treiman et al*., 2002]; more complex regions have darker shaded boxes, indicating higher fractal values.

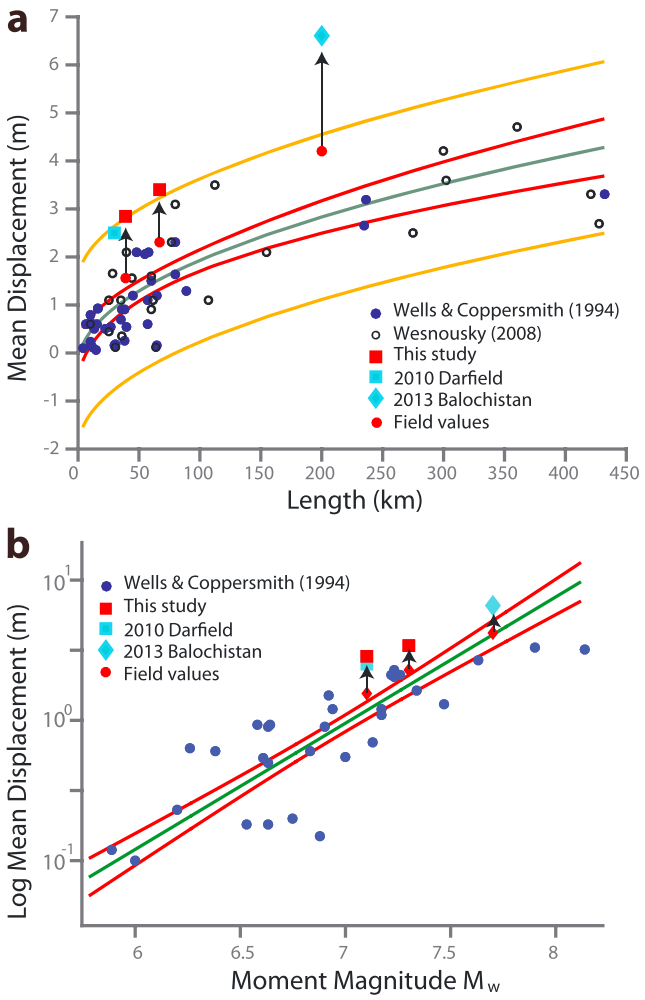

Figure 4. Surface rupture scaling relationships for large strike-slip earthquakes. (a) D_{mean} versus surface rupture length, with black circles from *Wesnousky* [2008], blue circles from *Wells and Coppersmith* [1994], red squares from this study, red circles showing field surveys of *Sieh et al.* [1993] and *Treiman et al.* [2002], cyan square from 2010 Darfield rupture [*Quigley et al.*, 2012], and cyan diamond from 2013 Balochistan earthquakes, which both include OFD, the latter having an "on-fault displacement" estimate [*Zinke et al.*, 2014]. Green line shows power law regression from *Wesnousky* [2008] with 95% confidence intervals (orange lines) and regression intervals (red lines). (b) D_{mean} versus M_w scaling relation for strike-slip events from *Wells and Coppersmith* [1994], plotted same symbols (Figure 4a). Both plots with arrows illustrate the effect of missing OFD on the scaling relation.

length (RL) [e.g., *Wells and Coppersmith*, 1994; *Wesnousky*, 2008], which are used widely in understanding fault mechanics [*Scholz*, 2002], paleomagnitude estimation [*Biasi and Weldon*, 2006], and probabilistic seismic hazard analysis [*Field et al.*, 2014]. For example, our D_{mean} values for the 1992 Landers and 1999 Hector Mine earthquakes are 3.41 m and 2.84 m, respectively, significantly larger than the field equivalents of 2.3 m [*Sieh et al.*, 1993] and 1.56 m [*Treiman et al.*, 2002], respectively. Comparing our D_{mean} values (as well as those from the 2013 M_w 7.7 Balochistan and 2010 M_w 7.1 Darfield earthquakes which include OFD) with the field measured values (which are used to define the regressions), and measurements from other surface ruptures (Figure 4), illustrates the significant bias introduced by missing OFD. Using the empirical scaling relation between D_{mean} and M_w of *Wells and Coppersmith* [1994], we obtained seismic moments (M_o) of 2.35×10^{27} dyn cm ($M_w = 7.51$) and 1.84×10^{27} dyn cm ($M_w = 7.44$) for the Landers and Hector Mine ruptures, respectively (see supporting information for methodological details [*Kanamori and Hanks*, 1979]), 2.1 and 3.27 times larger than the known geodetic values [*Simons et al.*, 2002; *Fialko*, 2004]. Additionally, we also found significant mismatches of our D_{mean} values with those expected from the D_{mean}-RL regression [*Wesnousky*, 2008], where an F test rejects at the 5% confidence level that our observed D_{mean} values would be produced by the observed RL. Our new D_{mean} measurements highlight the problematic nature of existing regressions based on surface offsets that do not include OFD, which can result in significant overestimates of M_w and RL, key parameters used in probabilistic seismic hazard assessment. We expect that future D_{mean} measurements that incorporate OFD will lead to higher displacement-length ratios preferentially for immature fault systems, which typically accommodate more diffuse deformation, also consistent with the notion that less mature, intraplate faults generate larger stress drops [*Shaw and Scholz*, 2001; *Manighetti et al.*, 2007]. Measurements of the complete near-field, coseismic deformation pattern that can now be achieved by optical image correlation and lidar differencing, will lead to a more reliable understanding of faulting mechanics, the total width of distributed deformation that poses a hazard to the built environment, and assessment of how surface slip compares to that at seismogenic depths [e.g., *Xu et al.*, 2016].

Acknowledgments
This research was funded by the U.S. National Science Foundation (NSF EAR-1147436 grant to Dolan). We thank Jerry Treiman for his help acquiring additional field measurements of the Landers earthquake. Finally, we thank Ed Nissen and an anonymous reviewer for the helpful comments which greatly improved the manuscript. We thank the USGS for the EarthExplorer website (http://earthexplorer.usgs.gov/), which greatly simplified access to the aerial photographs used in this study. Data used in this study can be found in the supporting information (Tables S1-S6).

References

Agnew, D. C., S. Owen, Z. Shen, G. Anderson, J. Svarc, H. Johnson, K. E. Austin, and R. Reilinger (2002), Coseismic displacements from the Hector Mine, California, earthquake: Results from survey-mode global positioning system measurements, *Bull. Seismol. Soc. Am.*, *92*, 1355–1364.

Ayoub, F., S. Leprince, and J. Avouac (2009), Co-registration and correlation of aerial photographs for ground deformation measurements, *ISPRS J. Photogramm. Remote Sens.*, *64*, 551–560.

Bennett, R., B. Wernicke, N. Niemi, A. Friedrich, and J. Davis (2003), Contemporary strain rates in the northern basin and range province from GPS data, *Tectonics*, *22*(2), 1008, doi:10.1029/2001TC001355.

Ben-Zion, Y., and C. G. Sammis (2003), Characterization of fault zones, *Pure Appl. Geophys.*, *160*, 677–715.

Biasi, G. P., and R. J. Weldon (2006), Estimating surface rupture length and magnitude of paleoearthquakes from point measurements of rupture displacement, *Bull. Seismol. Soc. Am.*, *96*, 1612–1623.

Bruhn, R. L., W. T. Parry, W. A. Yonkee, and T. Thompson (1994), Fracturing and hydrothermal alteration in normal fault zones, *Pure Appl. Geophys.*, *142*, 609–644.

Bryant, W. (1992), Surface fault rupture along the Johnson Valley, Homestead Valley, and related faults associated with the M_s 7.5 28 June 1992 Landers earthquake Fault Eval.Rept.FER-234, Calif. Div. Mines Geol.

Chen, T., S. Akciz, K. Hudnut, D. Zhang, and J. Stock (2015), Fault-slip distribution of the 1999 M_w 7.1 Hector Mine earthquake, California, estimated from postearthquake airborne LiDAR data, *Bull. Seismol. Soc. Am.*, *105*, 776–790.

Chester, F., and J. Logan (1986), Implications for mechanical properties of brittle faults from observations of the Punchbowl fault zone, California, *Pure Appl. Geophys.*, *124*, 79–106.

Dolan, J. F., and B. D. Haravitch (2014), How well do surface slip measurements track slip at depth in large strike-slip earthquakes? The importance of fault structural maturity in controlling on-fault slip versus off-fault surface deformation, *Earth Planet. Sci. Lett.*, *388*, 38–47.

Dolan, J. F., D. D. Bowman, and C. G. Sammis (2007), Long-range and long-term fault interactions in Southern California, *Geology*, *35*, 855–858.

Fialko, Y. (2004), Probing the mechanical properties of seismically active crust with space geodesy: Study of the coseismic deformation due to the 1992 M_w7. 3 Landers (southern California) earthquake, *J. Geophys. Res.*, *109*, B03307, doi:10.1029/2003JB002756.

Field, E. H., R. J. Arrowsmith, G. P. Biasi, P. Bird, T. E. Dawson, K. R. Felzer, D. D. Jackson, K. M. Johnson, T. H. Jordan, and C. Madden (2014), Uniform California Earthquake Rupture Forecast, Version 3 (UCERF3)—The time-independent model, *Bull. Seismol. Soc. Am.*, *104*, 1122–1180.

Gold, R. D., N. G. Reitman, R. W. Briggs, W. D. Barnhart, G. P. Hayes, and E. Wilson (2015), On-and Off-fault deformation associated with the September 2013 M_W 7.7 Balochistan earthquake: Implications for geologic slip rate measurements, *Tectonophysics*, *660*, 65–78.

Hudnut, K., N. King, J. Galetzka, K. Stark, J. Behr, A. Aspiotes, S. Van Wyk, R. Moffitt, S. Dockter, and F. Wyatt (2002), Continuous GPS observations of postseismic deformation following the 16 October 1999 Hector Mine, California, earthquake (M_w 7.1), *Bull. Seismol. Soc. Am.*, *92*, 1403–1422.

Jachens, R., V. Langenheim, and J. Matti (2002), Relationship of the 1999 Hector Mine and 1992 Landers fault ruptures to offsets on Neogene faults and distribution of late Cenozoic basins in the Eastern California shear zone, *Bull. Seismol. Soc. Am.*, *92*, 1592–1605.

Jacobs, A., D. Sandwell, Y. Fialko, and L. Sichoix (2002), The 1999 (M_w 7.1) Hector Mine, California, earthquake: Near-field postseismic deformation from ERS interferometry, *Bull. Seismol. Soc. Am.*, *92*, 1433–1442.

Kanamori, H., and T. Hanks (1979), A moment magnitude scale, *J. Geophys. Res.*, *84*, 2348–2349, doi:10.1029/JB084iB11p06131.

Leprince, S., F. Ayoub, Y. Klinger, and J. Avouac (2007a), Co-registration of optically sensed images and correlation (COSI-Corr): An operational methodology for ground deformation measurements paper presented at IEEE International Geoscience and Remote Sensing Symposium (IGARSS 2007), Barcelona, Spain.

Leprince, S., S. Barbot, F. Ayoub, and J. Avouac (2007b), Automatic and precise orthorectification, coregistration, and subpixel correlation of satellite images, application to ground deformation measurements, *IEEE Trans. Geosci. Remote Sens.*, *45*, 1529–1558.

Manighetti, I., M. Campillo, S. Bouley, and F. Cotton (2007), Earthquake scaling, fault segmentation, and structural maturity, *Earth Planet. Sci. Lett.*, *253*, 429–438.

McGill, S. F., and C. M. Rubin (1999), Surficial slip distribution on the central Emerson fault during the June 28, 1992, Landers earthquake, California, *J. Geophys. Res.*, *104*, 4811–4833, doi:10.1029/98JB01556.

Meade, B. J., and B. H. Hager (2005), Block models of crustal motion in southern California constrained by GPS measurements, *J. Geophys. Res.*, *110*, B03403, doi:10.1029/2004JB003209.

Michel, R., and J. Avouac (2006), Coseismic surface deformation from air photos: The Kickapoo step over in the 1992 Landers rupture, *J. Geophys. Res.*, *111*, B03408, doi:10.1029/2005JB003776.

Milliner, C. W., J. F. Dolan, J. Hollingsworth, S. Leprince, F. Ayoub, and C. Sammis (2015), Quantifying near-field and off-fault deformation patterns of the 1992 M_w 7.3 Landers earthquake, *Geochem. Geophys. Geosyst.*, *16*, 1577–1598, doi:10.1002/2014GC005693.

Nelson, M. R., and C. H. Jones (1987), Paleomagnetism and crustal rotations along a shear zone, Las Vegas, Southern Nevada, *Tectonics*, *6*, 13–33, doi:10.1029/TC006i001p00013.

Oskin, M., L. Perg, E. Shelef, M. Strane, E. Gurney, B. Singer, and X. Zhang (2008), Elevated shear zone loading rate during an earthquake cluster in Eastern California, *Geology*, *36*, 507–510.

Owen, S., G. Anderson, D. Agnew, H. Johnson, K. Hurst, R. Reilinger, Z. Shen, J. Svarc, and T. Baker (2002), Early postseismic deformation from the 16 October 1999 M_w 7.1 Hector Mine, California, earthquake as measured by survey-mode GPS, *Bull. Seismol. Soc. Am.*, *92*, 1423–1432.

Quigley, M., R. Van Dissen, N. Litchfield, P. Villamor, B. Duffy, D. Barrell, K. Furlong, T. Stahl, E. Bilderback, and D. Noble (2012), Surface rupture during the 2010 M_w 7.1 Darfield (Canterbury) earthquake: Implications for fault rupture dynamics and seismic-hazard analysis, *Geology*, *40*, 55–58.

Rockwell, T. K., S. Lindvall, T. Dawson, R. Langridge, W. Lettis, and Y. Klinger (2002), Lateral offsets on surveyed cultural features resulting from the 1999 Izmit and Düzce earthquakes, Turkey, *Bull. Seismol. Soc. Am.*, *92*, 79–94.

Scholz, C. H. (2002), *The Mechanics of Earthquakes and Faulting*, Cambridge Univ. Press, Cambridge, U. K.

Shaw, B. E., and C. H. Scholz (2001), Slip-length scaling in large earthquakes: Observations and theory and implications for earthquake physics, *Geophys. Res. Lett.*, *28*, 2995–2998, doi:10.1029/2000GL012762.

Shelef, E., and M. Oskin (2010), Deformation processes adjacent to active faults: Examples from eastern California, *J. Geophys. Res.*, *115*, B05308, doi:10.1029/2009JB006289.

Sibson, R. H. (2003), Thickness of the seismic slip zone, *Bull. Seismol. Soc. Am.*, *93*, 1169–1178.

Sieh, K., et al. (1993), Near-field investigations of the Landers earthquake sequence, April to July 1992, *Science*, *260*, 171–176.

Simons, M., Y. Fialko, and L. Rivera (2002), Coseismic deformation from the 1999 M_w 7.1 Hector Mine, California, earthquake as inferred from InSAR and GPS observations, *Bull. Seismol. Soc. Am.*, *92*, 1390–1402.

Teran, O. J., J. M. Fletcher, M. E. Oskin, T. K. Rockwell, K. W. Hudnut, R. M. Spelz, S. O. Akciz, A. P. Hernandez-Flores, and A. E. Morelan (2015), Geologic and structural controls on rupture zone fabric: A field-based study of the 2010 M_w 7.2 El Mayor–Cucapah earthquake surface rupture, *Geosphere*, *11*, 899–920.

Treiman, J. A., K. J. Kendrick, W. A. Bryant, T. K. Rockwell, and S. F. McGill (2002), Primary surface rupture associated with the M_w 7.1 16 1999 Hector Mine earthquake, San Bernardino, California, *Bull. Seismol. Soc. Am.*, *92*, 1171–1191.

Turcotte, D. L. (1997), *Fractals and Chaos in Geology and Geophysics*, Cambridge Univ. Press, Cambridge, U. K.

Wells, D. L., and K. J. Coppersmith (1994), New empirical relationships among magnitude, rupture length, rupture width, rupture area, and surface displacement, *Bull. Seismol. Soc. Am.*, *84*, 974–1002.

Wesnousky, S. G. (2008), Displacement and geometrical characteristics of earthquake surface ruptures: Issues and implications for seismic-hazard analysis and the process of earthquake rupture, *Bull. Seismol. Soc. Am.*, *98*, 1609–1632.

Xu, X., X. Tong, D. T. Sandwell, C. W. Milliner, J. F. Dolan, J. Hollingsworth, S. Leprince, and F. Ayoub (2016), Refining the shallow slip deficit, *Geophys. J. Int.*, *204*, 1867–1886.

Zinke, R., J. Hollingsworth, and J. F. Dolan (2014), Surface slip and off-fault deformation patterns in the 2013 M_W 7.7 Balochistan, Pakistan earthquake: Implications for controls on the distribution of near-surface coseismic slip, *Geochem. Geophys. Geosyst.*, *15*, 5034–5050, doi:10.1002/2014GC005538.